

CMB distortion anisotropies due to the decay of primordial magnetic fields

Koichi Miyamoto,^{1,*} Toyokazu Sekiguchi,^{2,3,†} Hiroyuki Tashiro,^{4,‡} and Shuichiro Yokoyama^{1,§}

¹*Institute for Cosmic Ray Research, The University of Tokyo, Kashiwa, Chiba, 277-8582, Japan*

²*Department of Physics, Nagoya University, Chikusa, Nagoya, 464-8602, Japan*

³*University of Helsinki and Helsinki Institute of Physics, P.O. Box 64, FI-00014, Helsinki, Finland*

⁴*Physics Department, Arizona State University, Tempe, AZ 85287, USA*

We investigate the power spectrum of the distortion of Cosmic Microwave Background (CMB) due to the decay of the primordial magnetic fields. It is known that there are two-types of the CMB distortions, so-called μ - and y -types and we find that the signal of the y -type distortion becomes larger than that of the μ -type one. We also discuss cross power spectra between the CMB distortions and the CMB temperature anisotropy, which are naturally generated due to the existence of the primordial magnetic fields. We find that such cross power spectra have small amplitudes compared with the auto-power spectra of the CMB distortions because of the Silk damping effect of the temperature anisotropy. We also investigate the possibility of detecting such signal in the future CMB experiments, including not only absolutely calibrated experiments such as PIXIE but also relatively calibrated experiments such as LiteBIRD and CMBpol.

I. INTRODUCTION

Recently, measurements of the Cosmic Microwave Background (CMB) spectral deviations from the black-body spectrum have become a focus of attention as important probes of the physics in the early Universe, because a powerful CMB observation missions called as PIXIE and PRISM have been proposed [1, 2]. Although the CMB spectrum is predicted as a nearly black-body spectrum in the standard Big Bang scenario, spectral distortions from the black-body spectrum can be created by energy injections into the CMB in the early universe. Therefore, the measurement of CMB distortions is expected as a probe of the thermal evolution of the Universe (for recent reviews, see Refs. [3, 4]). The diffusion of the acoustic waves before the recombination epoch, known as Silk damping [5], is one of the major energy injection sources [3, 6–12]. Other energy injection sources include massive unstable relic particles which decay before the recombination epoch [13], Hawking radiation from primordial black holes [14], diffusion damping of acoustic wave due to the cosmic strings [15, 16], and dissipation of primordial magnetic fields before and after the recombination epoch [17–19].

The CMB distortions are typically classified into two types, so-called μ - and y -distortions, depending on the epoch when energy injections occur. The μ -distortions are produced due to energy injections to CMB photons in the redshift range $2 \times 10^6 \gtrsim z \gtrsim 5 \times 10^4$. On the other hand, the y -distortions are created by energy injections in the redshift range $5 \times 10^4 \gtrsim z \gtrsim 1090$, and are also produced through the cosmic reionization process [20] and the thermal Sunyaev-Zel'dovich (SZ) effect [21] from the clusters of galaxies [22]. Current constraints on these distortions have been respectively obtained as $|\mu| < 9 \times 10^{-5}$ and $y < 1.5 \times 10^{-5}$ from COBE FIRAS [23]. The future mission PIXIE has the potential to give tighter constraints on both types of distortions, $|\mu| \sim 5 \times 10^{-8}$ and $y \sim 10^{-8}$ at the 5σ level [1], which will be improved further by an order of magnitude by another future survey PRISM.

In this paper, we investigate CMB distortions created by energy injections due to the damping of the primordial magnetic fields. Primordial magnetic fields could be the seed fields of observed micro-Gauss magnetic fields in the galaxies and galaxy clusters. There are a large number of works to study the origin of primordial magnetic fields in the early Universe; during inflation (see, e.g., [24–26] and references therein) or at the phase transition (see, e.g., [27–31] and references therein). Current upper limits on the large-scale magnetic fields are obtained through CMB anisotropies (see, e.g., [32–34]) and large scale structures (see, e.g., [34–36]). These upper limits allow the existence of the nano-Gauss primordial magnetic fields on Mpc scales. Recently, there are also several reports on the lower limits of magnetic fields in the inter-galactic medium whose strength is larger than $O(10^{-15} - 10^{-20})$ Gauss by using the observations of TeV blazars [37–40] although this claim is still under discussion [41, 42].

*Email: miyamone"at"icrr.u-tokyo.ac.jp

†Email: sekiguti"at"a.phys.nagoya-u.ac.jp

‡Email: hiroyuki.tashiro"at"asu.edu

§Email: shu"at"icrr.u-tokyo.ac.jp

The effect of primordial magnetic fields on the CMB distortions has been studied in Refs. [17–19]. If primordial magnetic fields exist, they induce the velocity of the photon-baryon fluid through the Lorentz force before the recombination epoch. The induced kinetic energy dissipates through the viscosity of the photon-baryon fluid corresponding to the Silk damping [43, 44]. Even after the recombination, the magnetic fields induce the velocity of baryon fluid via the Lorentz force with residual ionized baryons. This velocity fields also dissipate by ambipolar diffusion and decaying magnetohydrodynamical turbulence, and, consequently, CMB distortions are produced [18, 19]. For example, calculating spatially averaged distortions due to the magnetic field damping before the recombination epoch, the authors of Ref. [43] have obtained the upper limits on the strength of the magnetic fields by comparing the results from COBE-FIRAS, which are 3×10^{-8} Gauss on comoving coherent scale ~ 400 pc from the constraint for μ -distortions (0.3 pc for y -distortions). Recently, in Ref. [19], the authors have claimed that the PIXIE would be expected to give a constraint as 8×10^{-10} Gauss from the limit on $|\mu|$.

In this paper, we focus on the anisotropies of CMB distortions induced by primordial magnetic fields. In the future experiments, it is expected to measure such anisotropies of the distortion before the recombination epoch. We investigate the angular power spectrum of the μ - and y -distortions due to the damping of primordial magnetic fields with a given initial power spectrum. The shape of the angular power spectrum, in particular, the existence of the peak of the spectrum, is expected to depend on the kind of energy injections. We show that the amplitude of the spectrum depends on the structure of primordial magnetic fields and the peak scale informs us about the dissipation scale of magnetic fields.

We also evaluate the cross-correlation between the CMB distortion and the CMB temperature anisotropies. There are several works about such cross-correlation in the context of searching primordial non-Gaussianity [45, 46]. If the magnetic fields exist, for example, these fields generate the anisotropic stress during the radiation-dominated era which becomes a source of the additional primordial curvature perturbations. CMB temperature fluctuations induced by such primordial curvature perturbations sourced from the anisotropic stress of primordial magnetic fields would correlate with the CMB distortions due to the damping of primordial magnetic fields, because both of them are given in terms of the convolution of the magnetic fields. Including the analysis of such cross-correlation, we discuss the possibility of detecting the CMB distortions due to the existence of primordial magnetic fields.

This paper is organized as follows. In section 2, we briefly review CMB distortions induced from the damping of the magnetic fields and present the formalism for calculation of angular power spectra of anisotropies of μ and y parameters. We also discuss the cross-correlation between the CMB distortions and the CMB temperature anisotropy induced from the primordial magnetic fields. In section 3, we numerically calculate angular power spectra of the CMB distortions, taking the amplitude of the primordial magnetic fields to be a largest possible one derived from the current CMB observations. In section 4, we discuss the possibility of detecting anisotropic μ - and y -distortions in future or on-going CMB experiments. In section 5, we conclude this paper.

In this paper, we use the natural unit: $\hbar = c = k_B = 1$. Cosmological parameters are set according to WMAP result[47]: the abundance of baryon $\Omega_b = 0.045$, that of cold dark matter $\Omega_c = 0.222$, that of dark energy $\Omega_\Lambda = 0.733$ and Hubble constant $H_0 = 70.4$ km/s/Mpc.

II. FORMULATION FOR CMB DISTORTIONS DUE TO PRIMORDIAL MAGNETIC FIELDS

A. Primordial magnetic fields

We assume that spatially-varying random magnetic fields $\mathbf{B}(z, \mathbf{x})$ are created in the early universe. We define $\mathbf{b}(z, \mathbf{x})$ as

$$\mathbf{B}(z, \mathbf{x}) = \frac{\mathbf{b}(z, \mathbf{x})}{a^2}, \quad (1)$$

where a is the scale factor, and $\mathbf{b}(z, \mathbf{x})$ describes the evolution of magnetic fields other than decay due to cosmic expansion. In addition to the cosmic expansion, small-scale magnetic fields lose their amplitude through the dissipation process due to the viscous photon-baryon fluid before the recombination epoch [43]. Accordingly, the time-evolution of $\tilde{\mathbf{b}}(z, \mathbf{k})$, which is the Fourier transformed component of $\mathbf{b}(z, \mathbf{x})$ with comoving wavenumber \mathbf{k} , is given by

$$\tilde{\mathbf{b}}(z, \mathbf{k}) = \tilde{\mathbf{b}}(\mathbf{k}) \exp(-\tau(z, \mathbf{k})), \quad (2)$$

where

$$\tau(z, \mathbf{k}) = - \int_{t(z_0)}^{t(z)} dt' \Gamma(t', \mathbf{k}), \quad (3)$$

with the dissipation rate $\Gamma(t, \mathbf{k})$. Here, we take $z = z_0$ to be an arbitrary initial redshift when magnetic fields on interesting scales have hardly decayed yet and $\tilde{\mathbf{b}}(\mathbf{k}) = \tilde{\mathbf{b}}(z_0, \mathbf{k})$. Note that $\tau(z, k) > 1$ means that magnetic fields with wavenumber k have almost decayed at redshift z .

We assume that the initial random magnetic fields are isotropically homogeneous and obey the Gaussian statistics. Therefore, the auto-correlation function of $\tilde{\mathbf{b}}(\mathbf{k})$ is expressed as

$$\langle \tilde{b}_i(\mathbf{k}) \tilde{b}_j(\mathbf{p}) \rangle = P_{ij}(\hat{k}) P_B(k) (2\pi)^3 \delta(\mathbf{k} + \mathbf{p}), \quad (4)$$

where $k = |\mathbf{k}|$, $p = |\mathbf{p}|$ and

$$P_{ij}(\hat{k}) = \delta_{ij} - \hat{k}_i \hat{k}_j, \quad (5)$$

is a projection tensor which reflects the zero divergence of magnetic fields. We assume that the power spectrum, P_B , is given as a blue-tilted power-law function with a cut-off scale, defined as

$$P_B(k) = \begin{cases} n\pi^2 \frac{B_0^2}{k^3} \left(\frac{k}{k_c}\right)^n & ; k < k_c \\ 0 & ; k > k_c \end{cases}, \quad (6)$$

where $n > 0$ is the spectral index¹ and k_c is the cut-off wavenumber depending on the generation mechanism of the magnetic fields.

The dissipation rate $\Gamma(t, \mathbf{k})$ is expressed as the imaginary part in the solutions of dispersion relations for the magnetohydrodynamic (MHD) modes, called fast- and slow-magnetosonic, and Alfvén modes. In Ref. [43], the authors have shown that, among these modes, the Alfvén and slow-magnetosonic modes can survive below the Silk damping scale. Therefore the energy of the magnetic fields can be stored in these modes and dissipate with damping rates of the Alfvén and slow-magnetosonic modes, which depend on scales. On the scale larger than the mean free path for photon l_γ , i.e., $k/a \lesssim l_\gamma^{-1}$, the damping of MHD modes is caused by the photon shear viscosity. On the other hand, on the scale smaller than l_γ , i.e., $k/a \gtrsim l_\gamma^{-1}$, MHD modes are damped by the occasional collisions of the fluid particles with the background ones, which is parametrized by the drag coefficient $\alpha \simeq (l_\gamma R)^{-1}$ with $R = \frac{3\rho_b}{4\rho_r}$ being the ratio between the energy densities of the baryon ρ_b and the radiation ρ_r . Furthermore, the damping rate is different in the oscillatory limit and the overdamped limit and then the dissipation rate, depending on the scales, is obtained as [43]

$$\Gamma(t, \mathbf{k}) \sim \begin{cases} 0 & ; \text{for } \frac{k}{a} \lesssim H \quad (\text{no damping for superHubble modes}) \\ \frac{l_\gamma}{10(1+R)} \left(\frac{k}{a}\right)^2 & ; \text{for } H \lesssim \frac{k}{a} \lesssim \frac{30v_A \cos\theta(1+R)}{l_\gamma} \quad (\text{oscillatory limit for photon shear viscosity}) \\ \frac{v_A^2 \cos^2\theta}{5l_\gamma} & ; \text{for } \frac{30v_A \cos\theta(1+R)}{l_\gamma} \lesssim \frac{k}{a} \lesssim l_\gamma^{-1} \quad (\text{overdamped limit for photon shear viscosity}), \\ \frac{c_A^2 \cos^2\theta}{\alpha} \left(\frac{k}{a}\right)^2 & ; \text{for } l_\gamma^{-1} \lesssim \frac{k}{a} \lesssim \frac{\alpha}{2c_A \cos\theta} \quad (\text{overdamped limit for occasional collisions}) \\ \frac{\alpha}{2} & ; \text{for } \frac{k}{a} \gtrsim \frac{\alpha}{2c_A \cos\theta} \quad (\text{oscillatory limit for occasional collisions}) \end{cases}, \quad (7)$$

with

$$v_A^2 = \frac{\hat{\mathbf{B}}_{\text{eff}}^2}{(1+R+\hat{\mathbf{B}}_{\text{eff}}^2)}, \quad c_A^2 = \frac{\hat{\mathbf{B}}_{\text{eff}}^2}{R}. \quad (8)$$

Here H is the Hubble parameter, θ is the angle between $\hat{\mathbf{B}}_{\text{eff}}$ and \mathbf{k} , v_A and c_A respectively denote the relativistic and non-relativistic Alfvén velocities [43, 48, 49] and the normalized mean square of the effective background field $\hat{\mathbf{B}}_{\text{eff}}$ is given by

$$\hat{\mathbf{B}}_{\text{eff}}^2 \equiv \frac{\mathbf{B}_{\text{eff}}^2}{16\pi\rho_r/3} = \frac{\langle \mathbf{B}^2(z, \mathbf{x}) \rangle}{16\pi\rho_r/3} = \frac{3}{16\pi\rho_r} \int \frac{dk}{\pi^2} k^2 P_B(k) \frac{1}{a^4} e^{-2\tau(z,k)}. \quad (9)$$

We hereafter simply set as $\cos\theta = 1$, and regard $\tau(z, \mathbf{k})$ as the function of k .

¹ Although, here, we do not mention concrete models of generating the primordial magnetic fields, such blue-tilted power spectrum is motivated by some models, e.g., the phase transition scenarios in the early universe [27–31].

B. Auto- and cross-correlation functions of μ and y parameters

The dissipation of primordial magnetic fields discussed above can be a mechanism of energy injection which creates the CMB spectral distortions. Since the amplitude of magnetic fields spatially varies, the dissipation energy of the magnetic fields also spatially fluctuates and it can produce the anisotropic spectral distortions of the CMB.

The spectral distortions of the CMB are characterized by μ and y parameters. These parameters are given by [50, 51]

$$\mu(\mathbf{x}) = 1.4 \int_{z_{\mu,f}}^{z_{\mu,i}} dz \frac{dQ(z, \mathbf{x})/dz}{\rho_{\gamma}(z)}, \quad (10)$$

and

$$y(\mathbf{x}) = \frac{1}{4} \int_{z_{y,f}}^{z_{y,i}} dz \frac{dQ(z, \mathbf{x})/dz}{\rho_{\gamma}(z)}, \quad (11)$$

respectively. Here, $dQ(z, \mathbf{x})/dz$ is the energy injected at redshift z and comoving coordinate \mathbf{x} , $\rho_{\gamma}(z)$ is the photon energy density, and we take $z_{\mu,i} = 2 \times 10^6$, $z_{\mu,f} = z_{y,i} = 5 \times 10^4$ and $z_{y,f} = z_{\text{rec}} = 1090$. z_{rec} is also the redshift at the recombination.

The injected energy is given by [17]

$$\frac{dQ}{dz}(z, \mathbf{x}) = -\frac{1}{8\pi a^4} \frac{d}{dz} (\mathbf{b}(z, \mathbf{x}))^2. \quad (12)$$

Substituting Eq. (12) into Eqs. (10) and (11), μ and y parameters induced by dissipating magnetic fields are respectively given by

$$\mu(\mathbf{x}) = \frac{1.4}{8\pi} \left(\frac{(\mathbf{b}(z_{\mu,i}, \mathbf{x}))^2}{\rho_{\gamma,0}} - \frac{(\mathbf{b}(z_{\mu,f}, \mathbf{x}))^2}{\rho_{\gamma,0}} \right), \quad (13)$$

$$y(\mathbf{x}) = \frac{1}{32\pi} \left(\frac{(\mathbf{b}(z_{y,i}, \mathbf{x}))^2}{\rho_{\gamma,0}} - \frac{(\mathbf{b}(z_{y,f}, \mathbf{x}))^2}{\rho_{\gamma,0}} \right), \quad (14)$$

where $\rho_{\gamma,0} = \rho_{\gamma}(0)$. In terms of the Fourier modes of magnetic fields, $\tilde{\mathbf{b}}(z, \mathbf{k})$, we can rewrite these parameters as

$$\mu(\mathbf{x}) = \frac{1.4}{8\pi\rho_{\gamma,0}} \int \frac{d^3k}{(2\pi)^3} \int \frac{d^3k'}{(2\pi)^3} \tilde{\mathbf{b}}(\mathbf{k}) \cdot \tilde{\mathbf{b}}^*(\mathbf{k}') C_{\mu}(k, k') e^{i(\mathbf{k}-\mathbf{k}') \cdot \mathbf{x}}, \quad (15)$$

$$y(\mathbf{x}) = \frac{1}{32\pi\rho_{\gamma,0}} \int \frac{d^3k}{(2\pi)^3} \int \frac{d^3k'}{(2\pi)^3} \tilde{\mathbf{b}}(\mathbf{k}) \cdot \tilde{\mathbf{b}}^*(\mathbf{k}') C_y(k, k') e^{i(\mathbf{k}-\mathbf{k}') \cdot \mathbf{x}}, \quad (16)$$

where

$$C_{\mu}(k, k') = \exp(-\tau(z_{\mu,i}, k)) \exp(-\tau(z_{\mu,i}, k')) - \exp(-\tau(z_{\mu,f}, k)) \exp(-\tau(z_{\mu,f}, k')), \quad (17)$$

$$C_y(k, k') = \exp(-\tau(z_{y,i}, k)) \exp(-\tau(z_{y,i}, k')) - \exp(-\tau(z_{y,f}, k)) \exp(-\tau(z_{y,f}, k')). \quad (18)$$

Let us discuss the angular power spectrum of the distortions. First, considering the expansion of the distortion parameters, μ and y , by the spherical harmonics, $Y_{lm}(\hat{n})$, we can obtain each mode-coefficient as

$$a_{lm}^{\mu} = \int d^2\hat{n} \mu(r_{\text{rec}}\hat{n}) Y_{lm}^*(\hat{n}), \quad (19)$$

² Recently, Refs. [9, 19] found that an extra factor 1/3 in the Eqs. (10) and (11) is needed because only 1/3 of the energy injection contributes to the distortions. However this modification do not change our final results significantly.

and

$$a_{lm}^y = \int d^2\hat{n} y(r_{\text{rec}}\hat{n}) Y_{lm}^*(\hat{n}), \quad (20)$$

where we take the sudden last-scattering approximation in which the observed CMB photons are last-scattered simultaneously at $z = z_{\text{rec}}$. In Eqs. (19) and (20), \hat{n} is the direction of the line of sight and $r_{\text{rec}} = \int_0^{z_{\text{rec}}} dz/H(z) \simeq 1.4 \times 10^4$ Mpc is the comoving distance from the earth to the last-scattering surface. Angular power spectra of two kinds of distortions are given by

$$\langle a_{lm}^X (a_{l'm'}^Y)^* \rangle = C_l^{XY} \delta_{ll'} \delta_{mm'}, \quad (21)$$

where X and Y are either μ or y . According to Eqs. (4), (15), (16), (19) and (20), we have

$$C_l^{\mu\mu} = \frac{1.4^2}{2(2\pi)^5 \rho_{\gamma,0}^2} \int dp \int dq \int_{-1}^1 d\mu p^2 q^2 P_B(\chi) P_B(q) (C_\mu(\chi, q))^2 f(p, q, \mu) (j_l(pr_{\text{rec}}))^2, \quad (22)$$

$$C_l^{yy} = \frac{1}{32(2\pi)^5 \rho_{\gamma,0}^2} \int dp \int dq \int_{-1}^1 d\mu p^2 q^2 P_B(\chi) P_B(q) (C_y(\chi, q))^2 f(p, q, \mu) (j_l(pr_{\text{rec}}))^2, \quad (23)$$

and

$$C_l^{\mu y} = \frac{1.4}{8(2\pi)^5 \rho_{\gamma,0}^2} \int dp \int dq \int_{-1}^1 d\mu p^2 q^2 P_B(\chi) P_B(q) C_\mu(\chi, q) C_y(\chi, q) f(p, q, \mu) (j_l(pr_{\text{rec}}))^2, \quad (24)$$

where

$$\chi = \sqrt{p^2 + q^2 + 2pq\mu}, \quad f(p, q, \mu) = \frac{p^2(1 + \mu^2) + 4pq\mu + 2q^2}{p^2 + 2pq\mu + q^2}, \quad (25)$$

and j_l is the l -th spherical Bessel function.

Note that the finite thickness of the last scattering surface cannot be neglected for smaller scale anisotropies $l \gtrsim 1000$ and the sudden last-scattering approximation is not valid for such scales. According to Ref. [52], however, the effect of the finite thickness of the last scattering surface can be simply taken into account in the above expressions as

$$C_l^{XY} \approx \begin{cases} C_l^{XY,0} & ; \text{for } l < r_{\text{rec}}/\sigma_{\text{LS}} \\ \frac{C_l^{XY,0}}{l\sigma_{\text{LS}}/r_{\text{rec}}} & ; \text{for } l > r_{\text{rec}}/\sigma_{\text{LS}} \end{cases}, \quad (26)$$

where $C_l^{XY,0}$ is the angular power spectrum given by Eq. (22), (23) or (24) and $\sigma_{\text{LS}} \simeq 17$ Mpc [53] is the thickness of the last scattering surface.

C. Cross-correlation functions between CMB distortions and CMB temperature anisotropies

The cross correlation between the CMB temperature anisotropy and the CMB spectral distortion is exactly zero as long as the primordial curvature perturbations are pure Gaussian, and hence it would be a new probe of the non-Gaussian feature of the primordial curvature perturbations [45, 46]. Primordial magnetic fields generate not only CMB μ and y distortions as shown in the previous subsection, but also the large-scale temperature anisotropy of the CMB [32–34], which are in general given as a quadratic function of the random Gaussian magnetic fields, \mathbf{B} , as shown below. Since the μ and y parameters are also proportional to \mathbf{B}^2 as shown in Eqs. (13) and (14), the primordial magnetic fields can make non-zero cross-correlation between the CMB temperature and spectral distortion anisotropies. Therefore, we investigate such a cross-correlation as a signature of primordial magnetic fields in this section.

One of the effects of the primordial magnetic fields on the CMB temperature anisotropy is so-called a scalar passive mode,³ which is extra curvature perturbations induced from the magnetic anisotropic stress on super-horizon scales

³ There is also another type of CMB fluctuations called the scalar magnetic mode[54]. We will discuss this mode later and show that both of the cross-correlation angular power spectra due to the scalar passive mode and the scalar magnetic mode are far below the detectable level in future experiments in following sections. The cross-correlation angular power spectrum between the vector or tensor mode of the temperature anisotropy and the μ or y anisotropy vanishes, since μ and y are scalar-like quantities.

generated during radiation dominated era before the neutrino decoupling time. The scalar passive mode of the curvature perturbations on the comoving slicing, ζ_{sp} , is given by [54]

$$\zeta_{sp}(\mathbf{k}) = -\frac{1}{3}R_\gamma\Pi_B(\mathbf{k})\left(\ln\left(\frac{\eta_\nu}{\eta_B}\right) + \frac{5}{8R_\nu} - 1\right), \quad (27)$$

where Π_B is the scalar part of the anisotropic stress of magnetic fields, $R_\gamma = \rho_\gamma/\rho_r$, $\rho_r = \rho_\gamma + \rho_\nu$ is the energy density of relativistic particles, ρ_ν is the neutrino energy density, $R_\nu = \rho_\nu/\rho_r$, η_ν is the conformal time at neutrino decoupling and η_B is that at magnetic field generation. We hereafter set $\eta_\nu/\eta_B = 10^{17}$. This value corresponds to magnetic fields generated at the energy scale of Grand Unified Theory and maximizes the scalar passive mode. The scalar part of the anisotropic stress, Π_B , is given by

$$\Pi_B(\mathbf{k}) = \frac{9}{2}T_{ij}(\hat{k})\Delta^{ij}(\mathbf{k}), \quad (28)$$

where

$$\Delta^{ij}(\mathbf{k}) = \frac{1}{4\pi\rho_{\gamma,0}}\int\frac{d^3p}{(2\pi)^3}\int\frac{d^3q}{(2\pi)^3}\tilde{b}^i(\mathbf{p})\tilde{b}^j(\mathbf{q})(2\pi)^3\delta(\mathbf{k}-\mathbf{p}-\mathbf{q}), \quad (29)$$

and

$$T_{ij}(\hat{k}) = \hat{k}_i\hat{k}_j - \frac{1}{3}\delta_{ij}. \quad (30)$$

The multipole coefficient of the scalar passive mode is given in terms of ζ_{sp} as

$$a_{lm}^{T,sp} = 4\pi i^l \int\frac{d^3k}{(2\pi)^3}\Delta_l^S(k)\zeta_{sp}(\mathbf{k})Y_{lm}^*(\hat{k}), \quad (31)$$

where $\Delta_l^S(k)$ is the transfer function of the scalar mode which we calculate using CAMB [55, 56].

Then we can compute the cross-correlation angular power spectra between the CMB distortions and the CMB temperature anisotropies, which are defined as

$$\langle a_{lm}^X(a_{l'm'}^T)^* \rangle = C_l^{XT}\delta_{ll'}\delta_{mm'}, \quad (32)$$

where X is μ or y again. From Eqs (4), (15), (16), (19), (20), (27) and (31), explicit forms of C_l^{XT} are given by

$$C_l^{\mu T} = 1.4A\int dp\int dq\int_{-1}^1 d\mu p^2 q^2 P_B(\chi)P_B(q)C_\mu(q,\chi)\Delta_l^S(p)g(p,q,\mu)j_l(pr_{LS}), \quad (33)$$

and

$$C_l^{yT} = \frac{1}{4}A\int dp\int dq\int_{-1}^1 d\mu p^2 q^2 P_B(\chi)P_B(q)C_y(q,\chi)\Delta_l^S(p)g(p,q,\mu)j_l(pr_{LS}), \quad (34)$$

where

$$g(p,q,\mu) = \frac{(1-3\mu^2)k^2 - (1+\mu^2)p^2 - (1+3\mu^2)kp\mu}{3(k^2+p^2+2kp\mu)}, \quad (35)$$

and $A = \frac{1}{(2\pi)^5}\frac{3R_\gamma}{2\rho_{\gamma,0}^2}\left(\ln\left(\frac{\eta_\nu}{\eta_B}\right) + \frac{5}{8R_\nu} - 1\right)$.

III. ESTIMATE OF POWER SPECTRA OF THE CMB DISTORTION PARAMETERS

A. Current upper limit on primordial magnetic fields and scale of magnetic field decay

In order to evaluate the angular power spectra of the CMB distortion anisotropies derived in the previous section, we need to set parameters B_0 , n and k_c , which specify the power spectrum of primordial magnetic fields. In this

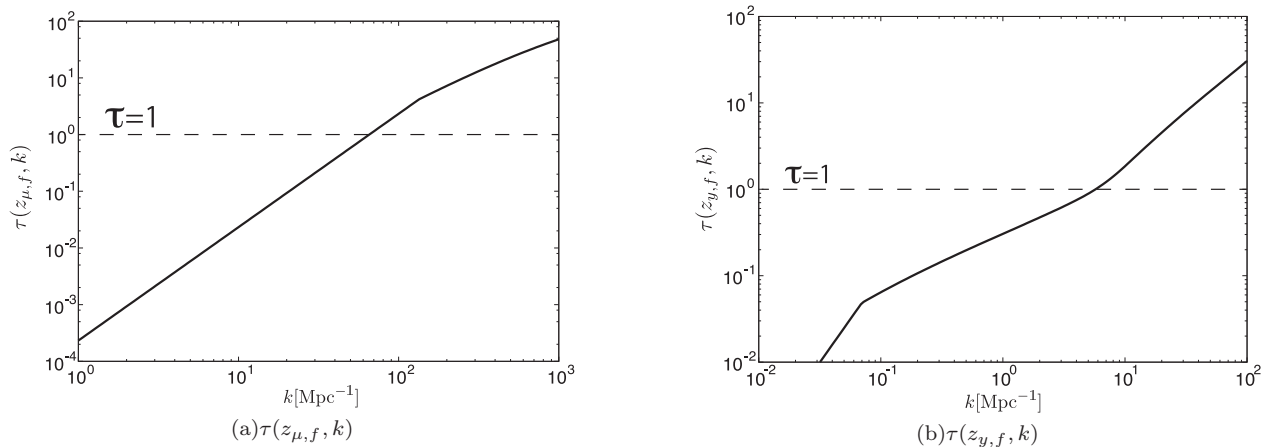


FIG. 1: The dependence of $\tau(z_{\mu,f}, k)$ and $\tau(z_{y,f}, k)$ on k . In both figures, we plot $B_0 = 1.1 \times 10^2$ nG, $n = 4$ and $k_c = 100 \text{ Mpc}^{-1}$ for $\tau(z_{\mu,f}, k)$ and $k_c = 10 \text{ Mpc}^{-1}$ for $\tau(z_{y,f}, k)$. The dashed line in each figure represents $\tau = 1$.

subsection, we briefly review the current constraints on these parameters. Then, in the next subsection, we consider situations where observational signals of μ and y anisotropies are maximized within such constraints.

One of strong cosmological constraints on primordial magnetic fields is that obtained from the isotropic CMB distortion by COBE FIRAS [23]: $|\mu| < 9 \times 10^{-5}$ and $y < 1.5 \times 10^{-5}$. These limits bring the upper bound of the decaying energy density of magnetic fields during the era when CMB distortions are created: $\rho_B = \mathbf{B}_{\text{eff}}^2/8\pi \lesssim 10^{-4} \times \rho_\gamma$ [17]. In terms of B_0 , this constraint leads

$$B_0 < 1.1 \times 10^2 \text{ nG}, \quad (36)$$

which is independent of n and k_c , if k_c is at the scale where magnetic fields decay while CMB distortions can be generated.

Another important constraint is that from observations of CMB temperature anisotropies. Ref. [57] derived the upper limit of the amplitude of primordial magnetic fields

$$|B_\lambda| < 3.0 \text{ nG}, \quad (37)$$

where B_λ corresponds to the strength of primordial magnetic fields on a comoving scale of 1 Mpc, which is related with B_0 as

$$B_0 = \left[\frac{2}{n\Gamma(n/2)} \right]^{1/2} (2\pi)^{n/2} \left(\frac{k_c}{k_\lambda} \right)^{n/2} B_\lambda, \quad (38)$$

with $k_\lambda = 2\pi \text{ Mpc}^{-1}$. From the above expression, we find that the constraint for B_0 obtained from the CMB temperature anisotropy depends on the spectral index n and the cut-off wavenumber k_c .

Our aim of this paper is to evaluate the maximum signals of the CMB distortion anisotropy due to primordial magnetic fields. Basically, the power spectrum of the CMB distortions due to the decay of the magnetic fields has a peak at the cut-off scale ($\sim 1/k_c$) and the peak amplitude depends on the total decaying energy density of magnetic fields over all scales, not only on the peak scale. Hence in order to obtain the large amplitude on the observable scales, which are much larger than the peak scale, we take the peak scale characterized by k_c as large as possible (We discuss the details in the next subsection). Since the typical scale of the decay of the magnetic fields becomes larger as the Universe expands, we set the peak scale of the power spectrum to the scale on which magnetic fields decay around the end of the production era of CMB distortions. This means that k_c satisfies $\tau(z_{\mu,f}, k_c) \sim 1$ for the μ -distortion and $\tau(z_{y,f}, k_c) \sim 1$ for the y -distortion. We plot $\tau(z_{\mu,f}, k)$ and $\tau(z_{y,f}, k)$ as functions of k in FIG. 1. In both figures, we take $B_0 = 1.1 \times 10^2$ nG and $n = 4$ which satisfy the COBE bound. According to FIG. 1, we set $k_c = 100 \text{ Mpc}^{-1}$ for the μ distortion and $k_c = 10 \text{ Mpc}^{-1}$ for y distortion. Note that $\tau(z_{X,f}, k) < 1$ for $k < k_c$ means that magnetic fields hardly decay during the production era of CMB distortions and C_l^{XX} is strongly suppressed. In FIG. 2, we show the region in the n - B_0 plane excluded by Eqs. (36) and (37), and we set the peak of the magnetic field power spectrum k_c as $k_c = 10 \text{ Mpc}^{-1}$ or $k_c = 100 \text{ Mpc}^{-1}$ for the constraint given by Eq. (37). The upper limit on B_0 from Eq. (36) does not depend on n , which is because of our notation (6). On the other hand, the constraint Eq. (37) becomes less

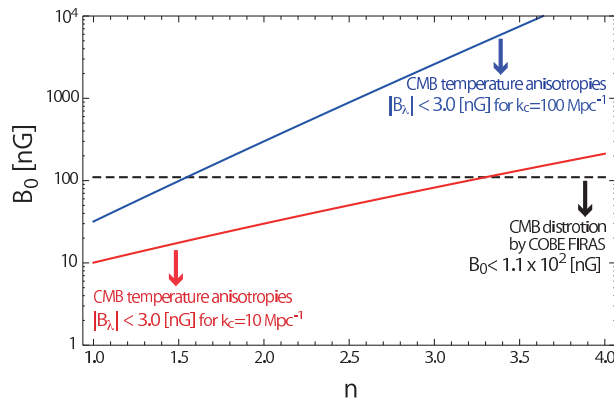


FIG. 2: The allowed region in the plane of B_0 , the amplitude of the magnetic field power spectrum, and n , its tilt. The black dashed line shows the upper bound given by Eq. (36), which is obtained from the observation of CMB distortion by COBE. The blue (red) line shows the constraint Eq. (37) from current observations of CMB temperature anisotropies for $k_c = 100(10) \text{ Mpc}^{-1}$.

severe as n increases, since for large n the magnetic field power spectrum is highly peaked at the scale smaller than that concerned with observable CMB anisotropies $k \lesssim k_\lambda$. Besides, the constraint Eq. (37) becomes looser for larger k_c , since the peak of the magnetic field power spectrum becomes apart from the CMB anisotropy scale. Eq. (37) is more severe than Eq. (36) for $n < 3.3$ and $n < 1.6$, when $k_c = 10 \text{ Mpc}^{-1}$ and $k_c = 100 \text{ Mpc}^{-1}$ respectively.

B. Angular power spectra of CMB distortions

Let us study angular power spectra of CMB distortion anisotropies.

1. Correlations of CMB distortions

First, we consider the auto- and cross-correlations in CMB distortions, i.e. μ - μ , y - y and μ - y . Here, we choose the parameter sets so that we obtain the maximum amplitude of the power spectra with the current constraint shown in FIG. 2 being satisfied. We show $C_l^{\mu\mu}$ in FIG. 3 for $n = 1$ (black solid), 2 (red long dashed) and 3 (blue short dashed), where we fix $k_c = 100 \text{ Mpc}^{-1}$. Following FIG. 2, we set B_0 to be a maximum allowed value for each n as 32 nG for $n = 1$ and $1.1 \times 10^2 \text{ nG}$ for $n = 2$ and $n = 3$. We also show C_l^{yy} in FIG. 4 for $n = 1$ (black solid), 2 (red long dashed), 3 (blue short dashed) and 4 (green dotted), where we fix $k_c = 10 \text{ Mpc}^{-1}$. As shown in FIG. 2, for $k_c = 10 \text{ Mpc}^{-1}$ the current observational cosmological limit for B_0 mainly comes from the CMB temperature anisotropies (denoted as the red line) for $n \lesssim 3.5$ and it depends on the spectral index n . Hence we set B_0 in FIG. 2 to be 10 nG, 29 nG, 83 nG and $1.1 \times 10^2 \text{ nG}$ for $n = 1, n = 2, n = 3$ and $n = 4$, respectively. As for the cross angular power spectrum, $C^{\mu y}$, which is shown in FIG. 5, we fix the amplitude B_0 to be $1.1 \times 10^2 \text{ nG}$ and change the peak scale k_c for each spectral index n . Following the observational constraint from the CMB temperature anisotropies given by Eq. (37) and the relation between B_λ and B_0 given by Eq. (38), for fixed B_0 , the peak scale k_c for each n is chosen in order to obtain the maximum allowed value of B_λ . Then, in this figure, we set k_c to 300, 100, 30, 10 Mpc^{-1} for $n = 1.2$ (black solid), 1.6 (red long dashed), 2.1 (blue short dashed) and 3.6 (green dotted), respectively.

The magnitudes of the auto-correlation spectra $C_l^{\mu\mu}$ and C_l^{yy} can be roughly estimated as follows. C_X given by Eqs. (17) or (18) is

$$C_X(k, k') \sim \begin{cases} 1 & ; \text{for } k_{X,f} < \max\{k, k'\} < k_{X,i} \\ 0 & ; \text{otherwise} \end{cases}, \quad (39)$$

where $k_{X,i}$ and $k_{X,f}$ the Fourier modes of magnetic fields which satisfies $\tau(k_{X,i}, z_{X,i}) = 1$ and $\tau(k_{X,f}, z_{X,f}) = 1$, respectively. In this sense, k_c is almost identical to $k_{X,f}$ here. The spherical Bessel function can be approximated as

$$j_l(x) \simeq \begin{cases} 0 & ; \text{for } x < l \\ \frac{1}{x} \cos\left(x - \frac{(l+1)\pi}{2}\right) & ; \text{for } x > l \end{cases}. \quad (40)$$

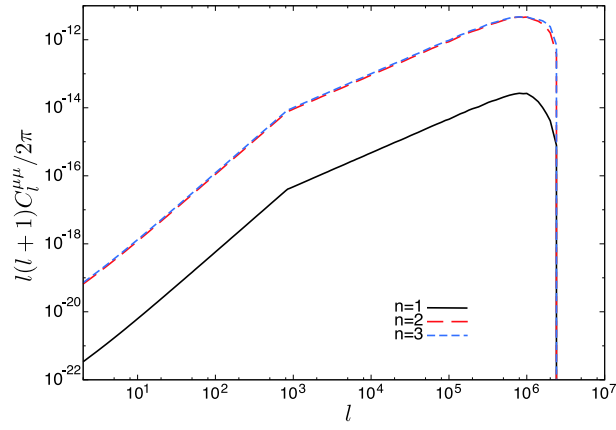


FIG. 3: The μ - μ auto-correlation angular power spectra for $n = 1$ (black solid), $n = 2$ (red long dashed) and $n = 3$ (blue short dashed). For all cases, $k_c = 100 \text{ Mpc}^{-1}$. B_0 is set to $B_0 = 32 \text{ nG}$ for $n = 1$, which corresponds to $B_\lambda = 3.0 \text{ nG}$, and $B_0 = 1.1 \times 10^2 \text{ nG}$ for $n = 2, 3$.

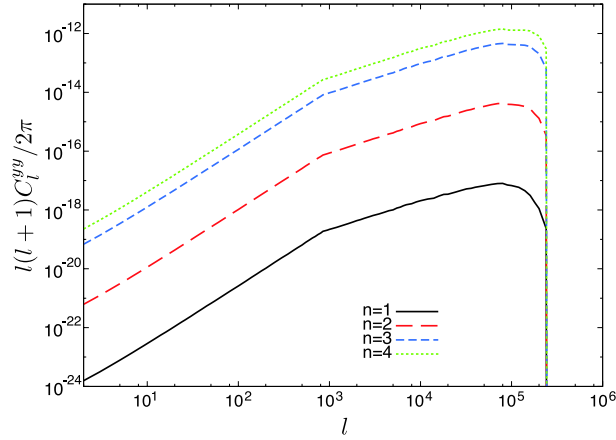


FIG. 4: The y - y auto-correlation angular power spectra for $n = 1$ (black solid), $n = 2$ (red long dashed), $n = 3$ (blue short dashed) and $n = 4$ (green dotted). For all cases, $k_c = 10 \text{ Mpc}^{-1}$. B_0 is set to $B_0 = 10 \text{ nG}$, 29 nG and 83 nG for $n = 1, 2$ and 3 respectively, which corresponds to $B_\lambda = 3.0 \text{ nG}$, and $B_0 = 1.1 \times 10^2 \text{ nG}$ for $n = 4$.

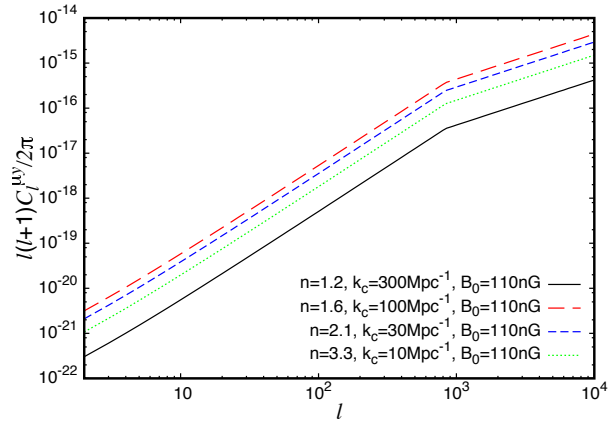


FIG. 5: The μ - y cross-correlation angular power spectra for parameter sets $(n, k_c [\text{Mpc}^{-1}]) = (1.2, 300)$ (black solid), $(1.6, 100)$ (red long dashed), $(2.1, 30)$ (blue short dashed) and $(3.3, 10)$ (green dotted). For all cases, B_0 is fixed to $1.1 \times 10^2 \text{ nG}$.

Neglecting the effect of the finite thickness of the last scattering surface, the auto-correlation spectrum C_l^{XX} can be roughly estimated as

$$\frac{l(l+1)C_l^{XX}}{2\pi} \sim \left(\frac{\rho_B}{\rho_\gamma}\right)^2 \frac{l^2}{(k_c r_{\text{rec}})^2}, \quad (41)$$

if $k_{X,f} < k_c < k_{X,i}$. Since we are setting $k_c \sim k_{X,f}$ as mentioned before, this estimation is consistent with the spectra shown in FIGs. 3 and 4, especially with respect to the dependence on l , $l(l+1)C_l^{XX}/2\pi \propto l^2$, for $l \lesssim 10^3$. The reason why $l(l+1)C_l^{XX}/2\pi \propto l$ for $l \gtrsim 10^3$ in FIGs. 3 and 4 is that the effect of the finite thickness of the last scattering surface, which is introduced as Eq. (26), suppresses C_l^{XX} by a factor $l\sigma_{\text{LS}}/r_{\text{rec}}$. The peak and the cut-off of $l(l+1)C_l^{XX}/2\pi$ at $l \sim 10^6$ for μ and at $l \sim 10^5$ for y correspond to those of the magnetic fields power spectrum at $k = k_c$.

Eq. (41) shows that the amplitude of C_l^{XX} is determined by the total energy of decaying magnetic fields. Therefore, for fixed k_c , its amplitude is determined only by B_0 , not by n . Since, here, we set B_0 to a smaller value for $n = 1$ than for $n = 2$ and $n = 3$ for $C_l^{\mu\mu}$ in order to satisfy the current observational constraints, the amplitude becomes also smaller. Of course, $C_l^{\mu\mu}$ for $n = 2$ and $n = 3$ overlaps each other because of the same value of B_0 for both cases. On the other hand, the amplitude of C_l^{yy} apparently seems to depend on the spectral index n in FIG. 4. However, since for C_l^{yy} we take smaller k_c than that for $C_l^{\mu\mu}$, the value of B_0 taken here strongly depends on the spectral index n in order to maximize the amplitude within the observational constraints shown in FIG. 2, as we have shown above. In the range of $n < 3.3$, B_0 is smaller for smaller n and hence the amplitude of C_l^{yy} becomes smaller for smaller B_0 , which is consistent with the simple estimation Eq. (41).

The second factor of the RHS of Eq. (41), which comes from the spherical Bessel function, tells us that smaller k_c leads to larger C_l^{XX} for fixed l , as mentioned in the previous subsection. In fact, $r_{\text{rec}} \simeq 10^4 \text{ Mpc}^{-1}$ and we take $k_c = 10 \text{ Mpc}^{-1}$ for μ and 100 Mpc^{-1} for y here, and hence, for the CMB observation scales ($l \lesssim 10^4$), C_l^{XX} is much suppressed compared with the value at the peak scale, $l \sim k_c r_{\text{rec}}$. This suppression reflects the fact that the typical scales of fluctuations of the μ - and y -parameter, $\sim 2\pi/k_c \sim 2\pi/k_{X,f}$, are much smaller than the observation scale, $\sim r_{\text{rec}}/l$. Because we take smaller k_c for C_l^{yy} compared with $C_l^{\mu\mu}$, the amplitude of C_l^{yy} seems to be larger than that of $C_l^{\mu\mu}$ for fixed l and the same value of B_0 .

On the other hand, as is shown in FIG. 5, we found that the cross-correlation spectrum $C_l^{\mu y}$ in general cannot be as large as the auto-correlation ones $C_l^{\mu\mu}$ and C_l^{yy} even if parameters (n, k_c, B_0) are tuned. This is because the scales of primordial magnetic fields which mainly contribute to μ - and y -type distortions are different. In other words, this can be understood by seeing that $C_\mu(\chi, q)C_y(\chi, q)$ in Eq.(24) vanishes, provided the rough approximation Eq. (39). We thus conclude that it is difficult to observe $C_l^{\mu y}$ unless $C_l^{\mu\mu}$ and C_l^{yy} are observed with high significance. Therefore we do not take into account $C_l^{\mu y}$ in Section IV, where we discuss detectability of primordial magnetic fields by CMB observations of distortion power spectra.

2. Cross-correlation with CMB temperature anisotropies

Next, we calculate the cross-correlation between CMB distortion anisotropies and the scalar passive mode of CMB temperature anisotropies given by Eqs. (33) and (34). We show $C_l^{\mu T}$ in FIG. 6 for $n = 1$ (black), 2 (red long dashed) and 3 (blue short dashed). For all cases, we set $k_c = 100 \text{ Mpc}^{-1}$ and $B_0 = 32 \text{ nG}$ for $n = 1$, which corresponds to $B_\lambda = 3.0 \text{ nG}$, and $B_0 = 1.1 \times 10^2 \text{ nG}$ for $n = 2, 3$ respectively. We also show C_l^{yT} in FIG. 7 for $n = 1$ (black), 2 (red long dashed) and 3 (blue short dashed). We take $k_c = 10 \text{ Mpc}^{-1}$ and $B_0 = 10 \text{ nG}, 29 \text{ nG}$ and 83 nG for $n = 1, 2$ and 3, respectively. As shown in FIGs. 6 and 7, $C_l^{\mu T}$ and C_l^{yT} are suppressed compared with the auto-correlations $C_l^{\mu\mu}$ and C_l^{yy} . This is just because the typical length scale of the CMB distortion fluctuations is much smaller than the Silk damping scale $k_{\text{Silk}} \sim 0.1 \text{ Mpc}^{-1}$. As is well known, the CMB temperature fluctuations have been exponentially damped by the Silk damping [58] on the scales with $k > k_{\text{Silk}}$. On the other hand, the amplitudes of the anisotropies of μ and y on the CMB observation scales ($k < k_{\text{Silk}}$), where the CMB temperature anisotropy keeps its amplitude, are much suppressed as shown in the above discussion about the auto power spectra of μ and y . Hence, even though the cross correlations between the temperature and distortion anisotropies exist due to the fact that both of these anisotropies are given in terms of the convolution of the Gaussian magnetic fields, the cross correlations are more suppressed than auto correlations of those anisotropies. Note that as shown in FIGs. 6 and 7, the amplitudes of the cross-correlations depend on not only B_0 but also n in contrast with the case of auto power spectra of μ and y . This is because the μ and y anisotropies on the scales larger than the Silk scale ($k < k_{\text{Silk}}$) depend on not only B_0 , which determines the amplitudes of μ and y anisotropies on the peak scale $\sim 2\pi/k_c$, but also the tilt n .

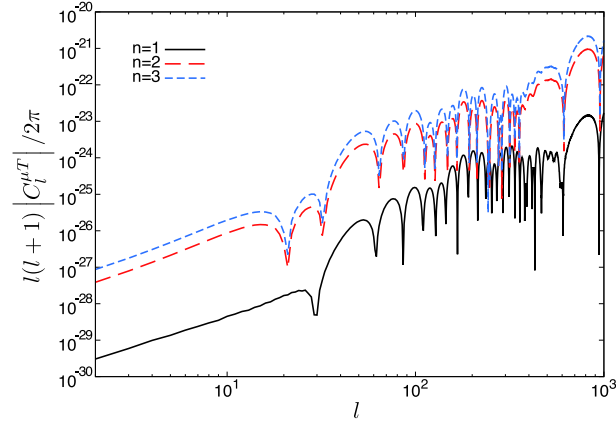


FIG. 6: The μ - T cross-correlation angular power spectra for $n = 1$ (black solid), $n = 2$ (red long dashed) and $n = 3$ (blue short dashed). For all cases, $k_c = 100 \text{ Mpc}^{-1}$. B_0 is set to $B_0 = 32 \text{ nG}$ for $n = 1$, and $B_0 = 1.1 \times 10^2 \text{ nG}$ for $n = 2, 3$.

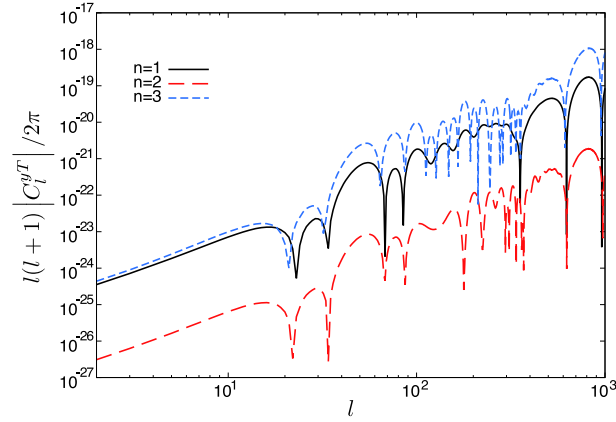


FIG. 7: The y - T cross-correlation angular power spectra for $n = 1$ (black solid), $n = 2$ (red long dashed) and $n = 3$ (blue short dashed). For all cases, $k_c = 10 \text{ Mpc}^{-1}$. B_0 is set to $B_0 = 10 \text{ nG}$, 29 nG and 83 nG for $n = 1, 2$ and 3 respectively, which corresponds to $B_\lambda = 3.0 \text{ nG}$.

IV. DETECTABILITY OF CMB DISTORTION ANISOTROPIES

In this section, we study the detectability of the anisotropies of CMB distortion parameters in the future observations by performing a signal-to-noise (SN) analysis. In order to evaluate SN ratio (SNR), first, we must estimate the variance of the angular power spectrum. The variances of $C_l^{\mu\mu}$ and C_l^{yy} estimated from the full sky observation of CMB are given by [59]

$$\sigma_{l'}^2 = \langle (C_l^{XX} - \langle C_l^{XX} \rangle) (C_{l'}^{XX} - \langle C_{l'}^{XX} \rangle) \rangle = \frac{2}{2l+1} (C_l^{XX} + C_l^{XX,N})^2 \delta_{ll'}, \quad (42)$$

where $C_l^{XX,N}$ is the noise power spectrum of the observation. We assume that the foregrounds can be removed perfectly. In this assumption, the noise power spectrum $C_l^{XX,N}$ consists of the experimental noise power spectrum and can be written as [59]

$$C_l^{XX,N} = \sigma_X^2 \theta_b^2 b_l^{-2}, \quad (43)$$

where σ_X is the 1σ uncertainty in X per pixel, θ_b is the beam width and b_l is the so-called beam transfer function given by

$$b_l = \exp\left(-\frac{l^2 \theta_b^2}{16 \ln 2}\right). \quad (44)$$

From Eq. (43), we can obtain the SNR in a measurement of $C_l^{\mu\mu}$ and C_l^{yy} by

$$\left(\frac{S}{N}\right)^2 = \sum_l \frac{2l+1}{2} \frac{(C_l^{XX})^2}{(C_l^{XX} + C_l^{XX,N})^2}. \quad (45)$$

We define a function which represents the detectable level of the signal $l(l+1)C_l^{XX}/2\pi$, C_l^{DL} , as

$$C_l^{DL} = \frac{l(l+1)}{2\pi} \sqrt{\frac{2}{(2l+1)l}} C_l^{XX,N}. \quad (46)$$

The fact that $l(l+1)C_l^{XX}/2\pi > C_l^{DL}$ means that SNR becomes larger than 1.

When we take a logarithmically homogeneous binning of l with bin width $\Delta \ln l = 1$, there are l multipoles in a bin at l . Since different multipoles are independent, the noise level per each bin should be given by σ_u/\sqrt{l} . Therefore, the detectable level of $l(l+1)C_l^{XX}/2\pi$ is roughly given by Eq. (46).

For the cross-correlations, $C_l^{\mu T}$ and C_l^{yT} , the variance is obtained from

$$\sigma_{w'}^2 = \langle (C_l^{XT} - \langle C_l^{XT} \rangle) (C_l^{XT} - \langle C_l^{XT} \rangle) \rangle = \frac{1}{2l+1} (C_l^{XX} + C_l^{XX,N}) (C_l^{TT} + C_l^{TT,N}) \delta_w, \quad (47)$$

where C_l^{TT} is the primary CMB temperature power spectrum and $C_l^{TT,N}$ is the noise power spectrum for the CMB temperature observation. Here we assume that, compared with the CMB signal, the experimental noise is very small on scales of interest. Therefore, we can neglect the noise power spectrum. In this assumption, the SNR for the cross-correlations is given by

$$\left(\frac{S}{N}\right)^2 \simeq \sum_l (2l+1) \frac{(C_l^{XT})^2}{(C_l^{XX} + C_l^{XX,N}) C_l^{TT}}. \quad (48)$$

Let us discuss the detectability of anisotropic CMB distortions in each future experiment.

A. PIXIE case

PIXIE [1] is a recently proposed satellite for CMB observation, which can measure CMB distortion parameters to a very high accuracy. For PIXIE, the beam width is $\theta_b = 1.6^\circ$ and the 1σ uncertainty in μ and y parameters averaged over the full sky are $\delta\mu = 10^{-8}$ and $\delta y = 2 \times 10^{-9}$ respectively [1]. This leads to

$$C_l^{\mu\mu,N} = 1.3 \times 10^{-15} \times \exp\left(\frac{l^2}{84^2}\right), \quad (49)$$

and

$$C_l^{yy,N} = 5.0 \times 10^{-17} \times \exp\left(\frac{l^2}{84^2}\right). \quad (50)$$

In FIG. 8, we show the function of the detectable level, C_l^{DL} , of the auto power spectra of μ (left panel (a)) and y (right panel (b)) for each CMB experiment and the largest C_l^{XX} allowed by the current observations with a black dotted line. The detectable level function for PIXIE is shown as a function of the multipole l with a red solid line. Due to the exponential factor in Eqs. (49) and (50), PIXIE can measure only large scale anisotropies, which correspond to $l \lesssim 100$, and for both of μ and y distortions the black dashed line, which represents the largest signal allowed by the current observations, is much lower than the red line. As a result, it would be difficult to detect the auto-correlation signals of the CMB distortion anisotropies induced by primordial magnetic fields by PIXIE.

The cross-correlation signals between CMB distortion and temperature anisotropies would be more difficult to be detected by PIXIE. A rough estimate gives $l(l+1)C_l^{TT} \sim 6.0 \times 10^{-10}$ as in [45], and we see that it is necessary that $C_{l=100}^{\mu T} \gtrsim 10^{-16}$ or $C_{l=100}^{yT} \gtrsim 10^{-17}$ for the SNR larger than 1. Both of $C_l^{\mu T}$ and C_l^{yT} shown in FIGs. 6 and 7 are much smaller than these required values.

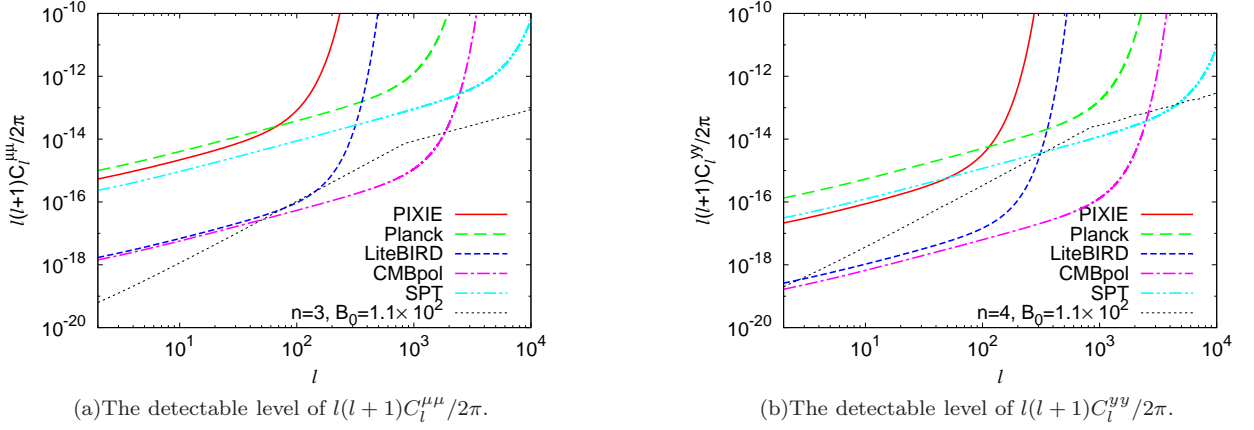


FIG. 8: The detectable levels of $l(l+1)C_l^{\mu\mu}/2\pi$ and $l(l+1)C_l^{yy}/2\pi$ in PIXIE (red solid), Planck (green long dashed), LiteBIRD (blue short dashed), CMBpol (magenta chain) and SPT (light blue two-dot chain). We also plot $l(l+1)C_l^{\mu\mu}/2\pi$ for $n=3, B_0=1.1 \times 10^2$ nG and $l(l+1)C_l^{yy}/2\pi$ for $n=4, B_0=1.1 \times 10^2$ nG for comparison (black dotted).

B. Planck case

The authors of [46] have argued that the anisotropies of CMB distortion parameters can be detected not only absolutely calibrated experiments such as PIXIE but also relatively calibrated experiments like WMAP and Planck, although an isotropic CMB distortion can be probed only by absolutely calibrated experiments. For relatively calibrated experiments, anisotropies of CMB distortion parameters are seen as temperature anisotropies, whose amplitude depends on the frequency channel. The temperature for photon frequency ν is given by

$$T(\nu) = \frac{T_0 x}{\ln(1+n(x))^{-1}}, \quad (51)$$

where $x = 2\pi\nu/T_0$, T_0 is the temperature averaged over all sky and $n(x)$ is the photon occupation number. Without CMB distortions, the occupation number is given by the Planck distribution as $n(x) = (e^x - 1)^{-1} \equiv n_0(x)$. Due to the CMB distortions the energy spectrum of CMB photons deviates from the Planck distribution. As a result, the apparent temperature anisotropy depending on the frequency channel is created from the CMB distortions. In the case of the μ -distortions, the apparent temperature anisotropy is given by [46]

$$\frac{\delta T(\hat{n}, \nu)}{T} \simeq -\frac{\delta\mu(\hat{n})}{x}, \quad (52)$$

where $\delta\mu$ is the fluctuating part of μ and $x = 2\pi\nu/T$. In the case of y -distortion, the resultant temperature anisotropy is

$$\frac{\delta T(\hat{n}, \nu)}{T} = \left(x \frac{e^x + 1}{e^x - 1} - 4 \right) \delta y(\hat{n}) \equiv a(\nu) \delta y(\hat{n}), \quad (53)$$

where δy is the fluctuating part of y . As shown in the above expressions, these temperature anisotropies produced by the CMB distortions have the frequency dependence, and taking difference between the temperature anisotropies in different frequency channels, we find $\delta\mu$ and δy . The experimental noise power spectrum in this type of observation using two different frequency channels ν_1 and ν_2 is given by

$$C_l^{\mu\mu, N} = \left[\frac{\nu_1 \nu_2 / (\nu_1 - \nu_2)}{56.80 \text{GHz}} \right]^2 \sum_{i=1,2} \sigma_{T,i}^2 \theta_{b,i}^2 b_{i,l}^{-2}, \quad (54)$$

for μ -distortions and

$$C_l^{yy, N} = \left(\frac{1}{a(\nu_1) - a(\nu_2)} \right)^2 \sum_{i=1,2} \sigma_{T,i}^2 \theta_{b,i}^2 b_{i,l}^{-2}, \quad (55)$$

(a) Planck (from [60])			(b) LiteBIRD (from [61])		
bands [GHz]	θ_b	σ_T	bands [GHz]	θ_b	σ_T
100	9.5'	2.5×10^{-6}	90	60'	2.1×10^{-8}
143	7.1'	2.2×10^{-6}	150	36'	3.3×10^{-8}
(c) CMBpol (from [62])			(d) SPT (from [63, 64])		
bands [GHz]	θ_b	σ_T	bands [GHz]	θ_b	σ_T
100	8'	1.1×10^{-7}	95	1.7'	9.6×10^{-6}
150	5'	1.6×10^{-7}	150	1.2'	5.5×10^{-6}

TABLE 1: Parameters which characterize sensitivities of various relatively calibrated experiments. θ_b is Gaussian beam width at FWHM, σ_T is temperature noise. Note that each satellite has some frequency bands other than those shown above. We here show parameters for two bands which have best sensitivities.

for y -distortions, where $\sigma_{T,i}$ is the 1σ uncertainty in $\delta T/T$ per pixel at frequency ν_i , $\theta_{b,i}$ is the beam width of channel ν_i and $b_{i,l} = \exp\left(-l^2\theta_{b,i}^2/16 \ln 2\right)$.

According to [60], Planck has the sensitivity $\sigma_T = 2.5 \times 10^{-6}$ with the beam width $\theta_b = 9.5'$ for 100 GHz channel and $\sigma_T = 2.2 \times 10^{-6}$ with $\theta_b = 7.1'$ for 143 GHz shown in TABLE 1(a). These channels have the best sensitivity among frequency channels of Planck. Therefore, the noise power spectrum for μ and y -distortions are

$$C_l^{\mu\mu,N} = 1.6 \times 10^{-15} \times e^{(l/855)^2} + 7.1 \times 10^{-16} \times e^{(l/1.1 \times 10^3)^2}, \quad (56)$$

and

$$C_l^{yy,N} = 2.2 \times 10^{-16} \times e^{(l/855)^2} + 9.4 \times 10^{-17} \times e^{(l/1.1 \times 10^3)^2}, \quad (57)$$

respectively. From the above expressions, we find that Planck is expected to probe the anisotropies on smaller scales compared with PIXIE due to the difference of exponential factor. However, as shown in FIG. 8 where C_l^{DL} for Planck is shown as a green long-dashed line, both of the largest allowed $C_l^{\mu\mu}$ and C_l^{yy} still do not have amplitudes large enough to be detected by Planck. Actually, $C_l^{\mu\mu}$ for $n = 3, B_0 = 1.1 \times 10^2 \text{ nG}$ gives $S/N \simeq 1.3 \times 10^{-2}$ and C_l^{yy} for $n = 4, B_0 = 1.1 \times 10^2 \text{ nG}$ gives $S/N \simeq 0.3$. For the cross-correlation cases, $C_l^{\mu T}$ and C_l^{yT} are far from the detectable level: $C_l^{\mu T} \gtrsim 10^{-18}$ and $C_l^{yT} \gtrsim 10^{-19}$ at $l \sim 10^3$.

C. LiteBIRD case

LiteBIRD [61] is a proposed CMB satellite which aims to detect low l B-mode polarization anisotropy. Although the angular resolution of LiteBIRD will be worse than Planck, the sensitivity per pixel will be better than Planck and it would be a powerful experiment to detect the CMB distortions through the relative calibration. For the beam width and sensitivity for the 90 GHz and the 150 GHz channels shown in TABLE 1(b), the experimental noise power spectrum for the relative calibration by LiteBIRD is given by

$$C_l^{\mu\mu,N} = 2.2 \times 10^{-18} \times e^{(l/135)^2} + 1.8 \times 10^{-18} \times e^{(l/226)^2}, \quad (58)$$

and

$$C_l^{yy,N} = 3.3 \times 10^{-19} \times e^{(l/135)^2} + 2.8 \times 10^{-19} \times e^{(l/226)^2}. \quad (59)$$

From the above expressions, we find that LiteBIRD can probe μ and y -distortion anisotropies with a sensitivity better than PIXIE up to as high l as PIXIE can. As a result, in an observation by LiteBIRD, anisotropies of CMB distortions induced by primordial magnetic fields can reach the detectable level within satisfying the current observational constraints, as shown in Fig. 8 where C_l^{DL} for LiteBIRD is shown as a blue short-dashed line. In particular, C_l^{yy} for $n = 3, B_0 = 1.1 \times 10^2 \text{ nG}$ gives $S/N \simeq 8$ and that for $n = 4, B_0 = 1.1 \times 10^2 \text{ nG}$ gives $S/N \simeq 22$. Approximating that C_l^{yy} depends on B_0 only through the overall factor proportional to B_0^4 ⁴ and setting the detection

⁴ Strictly speaking, B_0 affects C_l^{yy} also through $\text{Im}\omega(t, k)$ in Eq. (7).

threshold of the SNR to 4, we find the threshold value of B_0 for detection of C_l^{yy} . For $n \gtrsim 3$, magnetic fields with $B_0 > 70$ nG and $k_c = 10 \text{Mpc}^{-1}$ can generate detectable anisotropies of y -distortions. For a smaller value of n , C_l^{yy} can not be observable with the constraint Eq. (37) satisfied. $C_l^{\mu\mu}$ is slightly smaller than the detectable level ($C_l^{\mu\mu}$ for $n = 3, B_0 = 1.1 \times 10^2 \text{nG}$ gives $S/N \simeq 1.3$) and the cross correlations, $C_l^{\mu T}$ and C_l^{yT} , are still far too small to be detected by LiteBIRD.

D. CMBpol case

CMBpol [62] is a future CMB satellite with a sensitivity similar to LiteBIRD and an angular resolution higher than Planck. Using the 100GHz and 150GHz bands, whose beam width and sensitivity are given in TABLE 1(c), we evaluate each noise power spectrum of μ and y parameter as

$$C_l^{\mu\mu, N} = 1.6 \times 10^{-18} \times e^{(l/1.0 \times 10^3)^2} + 1.6 \times 10^{-18} \times e^{(l/1.6 \times 10^3)^2}, \quad (60)$$

and

$$C_l^{yy, N} = 1.9 \times 10^{-19} \times e^{(l/1.0 \times 10^3)^2} + 1.8 \times 10^{-19} \times e^{(l/1.6 \times 10^3)^2}. \quad (61)$$

Because of a high sensitivity and a high angular resolution, CMBpol enlarges the possibility to probe anisotropies of y -distortions, as shown in Fig. 8 where C_l^{DL} for CMBpol is shown as a magenta dot-dashed line. Setting the detection threshold of the SNR to 4 in a similar way to the LiteBIRD case, we find that the auto power spectrum of y anisotropies can be detected for the primordial magnetic fields with $n \gtrsim 3$, $B_0 > 39$ nG and $k_c = 10 \text{Mpc}^{-1}$. On the other hand, if the power spectrum of primordial magnetic fields is less blue-tilted, that is, $n \lesssim 2$, the primordial magnetic fields satisfying the current constraint Eq. (37) cannot induce detectable anisotropies of y . In CMBpol experiment, μ anisotropies can also reach the detectable level as shown in FIG. 8(a). For $n \gtrsim 2$, in particular, the primordial magnetic fields with $B_0 > 60$ nG and $k_c = 100 \text{Mpc}^{-1}$ create $C_l^{\mu\mu}$ detectable with a SNR larger than 4. However the smaller value of n makes μ anisotropies undetectable as in the case of y distortions. For the cross-correlation signals, $C_l^{\mu T}$ and C_l^{yT} still can not be detected by CMBpol.

E. SPT case

Angular power spectra of μ and y parameters induced by primordial magnetic fields have a larger amplitude on small scales as mentioned in the previous section, where space-based CMB experiments such as the above examples can not probe. CMB observations on such small scales $l > 1000$ are performed by ground-based telescopes. South Pole Telescope (SPT) [63] is one of the latest ones among such telescopes. According to [63, 64], SPT has $\sigma_T = 9.6 \times 10^{-6}$ and $\theta_b = 1.7'$ for the 95 GHz band and $\sigma_T = 5.5 \times 10^{-6}$ and $\theta_b = 1.2'$ for the 150 GHz band shown in TABLE 1(d). The noise power spectrum of SPT for each type of distortion is respectively given by

$$C_l^{\mu\mu, N} = 4.2 \times 10^{-16} \times e^{(l/4.8 \times 10^3)^2} + 7.6 \times 10^{-17} \times e^{(l/6.8 \times 10^3)^2}, \quad (62)$$

and

$$C_l^{yy, N} = 1.4 \times 10^{-17} \times e^{(l/4.8 \times 10^3)^2} + 1.0 \times 10^{-17} \times e^{(l/6.8 \times 10^3)^2}. \quad (63)$$

The detectable level, C_l^{DL} , for SPT is shown as a light blue two-dot chain line in FIG. 8. From FIG. 8(b), we can see that SPT can detect C_l^{yy} induced by the primordial magnetic fields, while as we will discuss shortly later contamination from the SZ effect would be significant. On the other hand, from FIG. 8(a), $C_l^{\mu\mu}$ induced from primordial magnetic fields satisfying the current observational constraints is too small to be detected by SPT.

F. Effects of the thermal Sunyaev-Zel'dovich effect

So far we have discussed the detectability of μ - and y -distortion anisotropies induced by primordial magnetic fields, simply assuming that there are no other sources of the distortions. However, these distortions can be generated by various processes both in the early and late-time Universe. In particular, as is mentioned in the introduction, y -distortion is generated by the thermal SZ effect in the late-time Universe. According to a recent measurement of y -distortion map by the Planck satellite [65], C_l^{yy} generated by the SZ effect is $\mathcal{O}(10^{-16})$ at $50 \lesssim \ell \lesssim 1000$. This is

about three order of magnitude larger than the maximum C_l^{yy} from primordial magnetic fields (See Fig. 8(b)). Since, at large angular scales, both C_l^{yy} from the thermal SZ effect and primordial magnetic fields have the same spectral shapes $C_l^{yy} \sim \text{constant}$, it should be difficult to detect the C_l^{yy} from primordial magnetic fields. However, at smaller scales, shapes of the spectra differ. In particular, C_l^{yy} of the thermal SZ effect drops sharply at around the angular scales of galaxy clusters, $l \sim 3000$, while one from primordial magnetic fields decays mildly as $C_l^{yy} \propto 1/l$. Thus, we expect future observations which observe C_l^{yy} at small angular scales may be able to distinguish primordial magnetic fields and the SZ effect. Furthermore, we also expect that the cross-correlation between thermal SZ effect and the distribution of galaxy clusters (see, e.g., Ref. [66]) helps us distinguish between the signals of y -distortion from the thermal SZ effect and the primordial magnetic fields considered here. On the other hand, since μ -distortions cannot be generated by astrophysical processes, we expect that it is more plausible to seek for the signature of primordial magnetic fields in the μ -distortion.

V. CONCLUSION

In this paper, we have considered μ - and y -distortions of the CMB photon energy spectrum, which are generated by decay of primordial magnetic fields. In particular, we have focused on anisotropies of the CMB distortions, which are induced by space-varying random magnetic fields. Using the decay rate of magnetic fields derived in [43], we have presented the formalism to calculate the angular power spectra of these distortion parameters. We have also considered the cross-correlations between the CMB distortion parameters and temperature anisotropies induced by magnetic fields.

We have numerically calculated angular power spectra $C_l^{\mu\mu}$, C_l^{yy} , $C_l^{\mu y}$, $C_l^{\mu T}$ and C_l^{yT} , taking various values of the tilt of the magnetic field power spectrum n . We have evaluated the maximum values of $C_l^{\mu\mu}$, C_l^{yy} , $C_l^{\mu y}$, $C_l^{\mu T}$ and C_l^{yT} allowed by the current observational constraints on the magnetic fields, setting the amplitude of the magnetic fields to the upper limit of the constraints and choosing the cut-off scales appropriately. The peak scales of the angular power spectra correspond to the cutoff scales of the magnetic fields and the peak amplitudes of the auto-correlation spectra $C_l^{\mu\mu}$ and C_l^{yy} are basically determined by the total energy density of the decay of the magnetic fields. However, since the angular power spectra have the dependence on l^2 , the amplitude are suppressed on the observation scales. On the other hand, we found that the cross correlation between the distortions $C_l^{\mu y}$ is small since different scales dominantly contributing to μ - and y -distortions are different. The cross-correlation with CMB temperature and distortion anisotropies, $C_l^{\mu T}$ and C_l^{yT} , are also suppressed more than $C_l^{\mu\mu}$ and C_l^{yy} , since temperature fluctuations on such a small length scale are exponentially suppressed due to Silk damping.

Following the numerical calculation of the angular power spectra, we have also discussed the possibility of detection of anisotropic CMB distortions induced by primordial magnetic fields. Although PIXIE is absolutely-calibrated experiment and have a high sensitivity for the measurement of the CMB distortions, it is not able to measure $C_l^{\mu\mu}$ and C_l^{yy} since it can reach the small scale only up to $l \sim 100$ in the current design. Following the method proposed in [46], relatively calibrated experiments can also measure anisotropies of CMB distortions. LiteBIRD can detect C_l^{yy} due to the magnetic fields with the large tilt $n \gtrsim 3$ and the amplitude close to the upper limit from current observations. CMBpol can measure C_l^{yy} by weaker magnetic fields. According to the situation, it might detect not C_l^{yy} but $C_l^{\mu\mu}$. Through observations of anisotropies of CMB distortions by these future CMB satellites, we might confirm existence of the primordial magnetic fields with highly blue-tilted power spectrum or put the novel constraint on such magnetic fields. On the other hand, $C_l^{\mu T}$ and C_l^{yT} are far from the detectable level in both observation. In small-scale CMB measurements by ground-based telescopes such as SPT, it is difficult to search anisotropies of CMB distortions due to magnetic fields. This is because the recent result of SPT is consistent with the SZ effect, which induces y -distortions indistinguishable from those by magnetic fields, and contributions from magnetic fields should be subdominant. This leads to the upper limit on magnetic fields: $B_0 < 1.8 \times 10^2$ nG for $k_c = 10$ Mpc $^{-1}$, which is larger by an $\mathcal{O}(1)$ factor than the COBE constraint, Eq. (36). The μ anisotropies are too small to be detected by SPT.

We mention to another contribution from primordial magnetic fields to the cross-correlation between CMB distortion and temperature anisotropies. In addition to the scalar passive mode considered here as the CMB temperature anisotropies sourced from the primordial magnetic fields, primordial magnetic fields also induce the so-called compensated scalar magnetic mode of CMB temperature fluctuations [54]. Although it is subdominant compared with the scalar passive mode for $l \lesssim 5000$ [54], it becomes the dominant component for higher l . This is because the scalar magnetic mode is actively produced and not suppressed exponentially like the scalar passive mode. Since small-scale perturbations also contribute to C_l^{XT} for small l , it could be possible that the scalar magnetic mode makes a considerable contribution to C_l^{XT} in the observable range with the blue-tilted power spectrum of the magnetic fields. As a brute-force estimation for such contribution, let us consider the unrealistic case where the exponential suppression due to the Silk damping is absent in the temperature anisotropies. In this case, we can expect from FIG. 2 in [54]

that the temperature anisotropy induced from the scalar passive mode is larger than that generated by the scalar magnetic mode by several orders of magnitude even on small scales. Furthermore, the angular cross power spectra between the temperature anisotropy induced from the scalar passive mode and the CMB distortions due to the primordial magnetic fields, C_l^{XT} , is expected to be comparable to the auto angular power spectrum of the temperature anisotropy, C_l^{TT} , in the absence of Silk damping. This is because Eqs. (22) and (33) (Eqs. (23) and (34)) have almost same forms except for the difference in $\mathcal{O}(1)$ prefactors when we make an approximation that $\Delta_l^S(k) \sim j_l(kr_{\text{rec}})$. We therefore see that C_l^{XT} due to the scalar magnetic mode would be smaller than C_l^{XX} by several orders of magnitudes. Hence, when we consider the detectability of the CMB distortions due to the primordial magnetic fields in the previous section, including C_l^{XT} due to the scalar magnetic mode in the analysis seems not to increase the detectability of the distortions. Then, we do not include the effects of the scalar magnetic mode in this paper and would like to consider the detailed analysis including such effect as a future issue.

Although PIXIE will not detect anisotropic parts of μ and y induced by primordial magnetic fields, it can detect their isotropic parts if $\mu \gtrsim 5 \times 10^{-8}$ or $y \gtrsim 10^{-8}$, which correspond to primordial magnetic fields with $\rho_B/\rho_\gamma \gtrsim 10^{-8}$ or $B_0 \gtrsim 1\text{nG}$. Combining the result of PIXIE with that of observations of μ and y anisotropies by other satellites, we might be able to confirm that the source of CMB distortions is primordial magnetic fields. Such a type of analysis will shed light on physics in the early Universe in a novel way.

Acknowledgments

S.Y. would like to thank Jens Chluba for useful discussion. K.M., S.Y. and T.S. would like to thank the Japan Society for the Promotion of Science for financial support. H.T. is supported by the DOE at the Arizona State University.

-
- [1] A. Kogut, D. J. Fixsen, D. T. Chuss, J. Dotson, E. Dwek, M. Halpern, G. F. Hinshaw and S. M. Meyer *et al.*, JCAP **1107**, 025 (2011) [arXiv:1105.2044 [astro-ph.CO]].
 - [2] P. Andre *et al.* [PRISM Collaboration], arXiv:1306.2259 [astro-ph.CO].
 - [3] J. Chluba and R. A. Sunyaev, arXiv:1109.6552 [astro-ph.CO].
 - [4] R. A. Sunyaev and R. Khatri, Int. J. Mod. Phys. D **22**, 1330014 (2013) [arXiv:1302.6553 [astro-ph.CO]].
 - [5] J. Silk, Astrophys. J. **151**, 459 (1968)
 - [6] J. D. Barrow and P. Coles, MNRAS, **248**, 52 (1991)
 - [7] R. A. Daly, Astrophys. J., **371**, 14 (1991)
 - [8] W. Hu, D. Scott and J. Silk, Astrophys.J., **430**, L5 (1994)
 - [9] J. Chluba, R. Khatri and R. A. Sunyaev, arXiv:1202.0057 [astro-ph.CO].
 - [10] J. B. Dent, D. A. Easson and H. Tashiro, Phys. Rev. D **86**, 023514 (2012) [arXiv:1202.6066 [astro-ph.CO]].
 - [11] R. Khatri and R. A. Sunyaev, JCAP **1206**, 038 (2012) [arXiv:1203.2601 [astro-ph.CO]].
 - [12] J. Chluba, A. L. Erickcek and I. Ben-Dayan, Astrophys. J. **758**, 76 (2012) [arXiv:1203.2681 [astro-ph.CO]].
 - [13] W. Hu and J. Silk, Phys. Rev. Lett. **70**, 2661 (1993).
 - [14] H. Tashiro and N. Sugiyama, Phys. Rev. D **78**, 023004 (2008) [arXiv:0801.3172 [astro-ph]].
 - [15] H. Tashiro, E. Sabancilar and T. Vachaspati, Phys. Rev. D **85**, 103522 (2012) [arXiv:1202.2474 [astro-ph.CO]].
 - [16] H. Tashiro, E. Sabancilar and T. Vachaspati, arXiv:1212.3283 [astro-ph.CO].
 - [17] K. Jedamzik, V. Katalinic and A. V. Olinto, Phys. Rev. Lett. **85**, 700 (2000) [astro-ph/9911100].
 - [18] S. K. Sethi and K. Subramanian, Mon. Not. Roy. Astron. Soc. **356**, 778 (2005) [astro-ph/0405413].
 - [19] K. E. Kunze and E. Komatsu, arXiv:1309.7994 [astro-ph.CO].
 - [20] W. Hu, D. Scott and J. Silk, Phys. Rev. D **49**, 648 (1994) [astro-ph/9305038].
 - [21] Y. . B. Zeldovich and R. A. Sunyaev, Astrophys. Space Sci. **4**, 301 (1969).
 - [22] A. Refregier, E. Komatsu, D. N. Spergel and U. -L. Pen, Phys. Rev. D **61**, 123001 (2000) [astro-ph/9912180].
 - [23] D. J. Fixsen, E. S. Cheng, J. M. Gales, J. C. Mather, R. A. Shafer and E. L. Wright, Astrophys. J. **473**, 576 (1996) [astro-ph/9605054].
 - [24] B. Ratra, Astrophys. J. **391**, L1 (1992).
 - [25] J. Martin and J. 'i. Yokoyama, JCAP **0801**, 025 (2008) [arXiv:0711.4307 [astro-ph]].
 - [26] V. Demozzi, V. Mukhanov and H. Rubinstein, JCAP **0908**, 025 (2009) [arXiv:0907.1030 [astro-ph.CO]].
 - [27] C. J. Hogan, Phys. Rev. Lett. **51**, 1488 (1983).
 - [28] T. Vachaspati, Phys. Lett. B **265**, 258 (1991).
 - [29] K. Enqvist and P. Olesen, Phys. Lett. B **329**, 195 (1994) [hep-ph/9402295].
 - [30] G. Sigl, A. V. Olinto and K. Jedamzik, Phys. Rev. D **55**, 4582 (1997) [astro-ph/9610201].
 - [31] T. Kahniashvili, A. G. Tevzadze, A. Brandenburg and A. Neronov, arXiv:1212.0596 [astro-ph.CO].
 - [32] M. Shiraishi, D. Nitta, S. Yokoyama and K. Ichiki, JCAP **1203**, 041 (2012) [arXiv:1201.0376 [astro-ph.CO]].

- [33] D. G. Yamazaki, T. Kajino, G. J. Mathew and K. Ichiki, Phys. Rept. **517**, 141 (2012) [arXiv:1204.3669 [astro-ph.CO]].
- [34] J. R. Shaw and A. Lewis, Phys. Rev. D **86**, 043510 (2012) [arXiv:1006.4242 [astro-ph.CO]].
- [35] K. L. Pandey and S. K. Sethi, Astrophys. J. **762**, 15 (2013) [arXiv:1210.3298 [astro-ph.CO]].
- [36] T. Kahniashvili, Y. Maravin, A. Natarajan, N. Battaglia and A. G. Tevzadze, Astrophys. J. **770**, 47 (2013) [arXiv:1211.2769 [astro-ph.CO]].
- [37] F. Tavecchio, G. Ghisellini, L. Foschini, G. Bonnoli, G. Ghirlanda and P. Coppi, Mon. Not. Roy. Astron. Soc. **406**, L70 (2010) [arXiv:1004.1329 [astro-ph.CO]].
- [38] A. Neronov and I. Vovk, Science **328**, 73 (2010) [arXiv:1006.3504 [astro-ph.HE]].
- [39] K. Dolag, M. Kachelriess, S. Ostapchenko and R. Tomas, Astrophys. J. **727**, L4 (2011) [arXiv:1009.1782 [astro-ph.HE]].
- [40] K. Takahashi, M. Mori, K. Ichiki and S. Inoue, arXiv:1103.3835 [astro-ph.CO].
- [41] A. E. Broderick, P. Chang and C. Pfommer, Astrophys. J. **752**, 22 (2012) [arXiv:1106.5494 [astro-ph.CO]].
- [42] F. Miniati and A. Elyiv, arXiv:1208.1761 [astro-ph.CO].
- [43] K. Jedamzik, V. Katalinic and A. V. Olinto, Phys. Rev. D **57**, 3264 (1998) [astro-ph/9606080].
- [44] K. Subramanian and J. D. Barrow, Phys. Rev. D **58**, 083502 (1998) [astro-ph/9712083].
- [45] E. Pajer and M. Zaldarriaga, Phys. Rev. Lett. **109**, 021302 (2012) [arXiv:1201.5375 [astro-ph.CO]].
- [46] J. Ganc and E. Komatsu, Phys. Rev. D **86**, 023518 (2012) [arXiv:1204.4241 [astro-ph.CO]].
- [47] G. Hinshaw, D. Larson, E. Komatsu, D. N. Spergel, C. L. Bennett, J. Dunkley, M. R. Nolte and M. Halpern *et al.*, arXiv:1212.5226 [astro-ph.CO].
- [48] T. R. Seshadri and K. Subramanian, Phys. Rev. Lett. **87**, 101301 (2001) [astro-ph/0012056].
- [49] A. Mack, T. Kahniashvili and A. Kosowsky, Phys. Rev. D **65**, 123004 (2002) [astro-ph/0105504].
- [50] R. A. Sunyaev and Y. B. Zeldovich, Ann. Rev. Astron. Astrophys. **18**, 537 (1980).
- [51] W. Hu and J. Silk, Phys. Rev. D **48**, 485 (1993).
- [52] K. Subramanian and J. D. Barrow, Phys. Rev. Lett. **81**, 3575 (1998) [astro-ph/9803261].
- [53] K. Subramanian and J. D. Barrow, Mon. Not. Roy. Astron. Soc. **335**, L57 (2002) [astro-ph/0205312].
- [54] J. R. Shaw and A. Lewis, Phys. Rev. D **81**, 043517 (2010) [arXiv:0911.2714 [astro-ph.CO]].
- [55] A. Lewis, A. Challinor and A. Lasenby, Astrophys. J. **538**, 473 (2000) [astro-ph/9911177].
- [56] <http://camb.info/>
- [57] D. G. Yamazaki, K. Ichiki, T. Kajino and G. J. Mathews, Phys. Rev. D **81**, 023008 (2010) [arXiv:1001.2012 [astro-ph.CO]].
- [58] J. Silk, Nature, **215**, 1155 (1972)
- [59] L. Knox, Phys. Rev. D **52**, 4307 (1995) [astro-ph/9504054].
- [60] [Planck Collaboration], astro-ph/0604069.
- [61] <http://cmbpol.kek.jp/litebird/>
- [62] D. Baumann *et al.* [CMBPol Study Team Collaboration], AIP Conf. Proc. **1141**, 10 (2009) [arXiv:0811.3919 [astro-ph]].
- [63] C. L. Reichardt, L. Shaw, O. Zahn, K. A. Aird, B. A. Benson, L. E. Bleem, J. E. Carlstrom and C. L. Chang *et al.*, Astrophys. J. **755**, 70 (2012) [arXiv:1111.0932 [astro-ph.CO]].
- [64] K. K. Schaffer, T. M. Crawford, K. A. Aird, B. A. Benson, L. E. Bleem, J. E. Carlstrom, C. L. Chang and H. M. Cho *et al.*, Astrophys. J. **743**, 90 (2011) [arXiv:1111.7245 [astro-ph.CO]].
- [65] P. A. R. Ade *et al.* [Planck Collaboration], arXiv:1303.5081 [astro-ph.CO].
- [66] W. Fang, K. Kadota and M. Takada, Phys. Rev. D **85**, 023007 (2012) [arXiv:1109.4934 [astro-ph.CO]].